KAPL-P-000163
(K97044)
CONF-970666--

STABILITY ANALYSIS OF IMPLICIT MULTI-FLUID SCHEMES

R. F. Kunz, W. K. Cope

June 1997

NOTICE

KAPL ATOMIC POWER LABORATORY SCHENECTADY, NEW YORK 10701

Operated for the U. S. Department of Energy
by KAPL, Inc. a Lockheed Martin company

DISCLAIMER

STABILITY ANALYSIS OF IMPLICIT MULTI-FLUID SCHEMES

R. F. Kunz, W. K. Cope
Lockheed Martin, Schenectady, NY 12301

S. Venkateswaran
The Pennsylvania State University, University Park, PA 16803

Abstract

A new implicit method has been developed for solving the viscous full multi-fluid equations, which incorporate transport and generation of mass and momentum for each component present in a system. This work presents stability analysis and application of the important full multi-fluid system in a fully implicit algorithm. The stability analyses presented demonstrate the performance of several iterative schemes applied to the solution of the linearized systems which arise in the formulation. These include block Jacobi and symmetric block Gauss-Siedel schemes with various preconditioners applied. A hierarchy of increasing physical complexity is pursued, starting with one-dimensional, two-fluid systems with minimum inter-field dynamic coupling and no mass transfer. These analyses are extended to systems employing physically important inter-field forces (drag, turbulence dispersion, virtual mass). The effects of mass transfer, multiple fields (i.e., $n\phi > 2$) and multiple dimensions are also considered. A two-fluid Navier-Stokes code has been developed based on this new scheme. Results are presented which verify the validity of the stability analyses presented for the coupled scheme.

Introduction

Multi-phase flows which require full multi-fluid modelling arise in a wide class of engineering problems, where non-equilibrium dynamics and thermodynamics of the interfaces between constituents play important roles in the evolution of the ensemble averaged mean flow. Examples include cyclone separators, two-phase flow in jets and curved ducts and boiling flow in heat exchangers. Though much CFD research to date has been performed for reacting flows, the interfacial dynamics and thermodynamics in many of these "aerodynamic" multi-constituent flows occur on such small spatial scales that mixture momentum and energy equations can be employed. For the many cases that such homogeneous mixture approximations are not valid, full two-fluid modelling is appropriate. There, separate equations for the transport and generation of mass, momentum and energy for each component present in a system are solved.

This level of modelling greatly complicates the numerics of the problem. To date, the appearance of numerical stability analysis of multi-fluid models in the CFD literature has been limited to several semi-implicit methods related to the Implicit Courant Eulerian (ICE) algorithm[1, 2, 3] and analyses focused on maximizing inter-field coupling in segregated pressure based methods[4, 5]. This work represents stability analysis and application of the important multi-dimensional full multi-fluid system in a fully implicit algorithm.

Theoretical Formulation

Governing Equations

In full multi-fluid formulations, independent equations are employed for the transport/generation of mass, momentum and energy for each field present in a system. The ensemble averaged governing equations for steady state, one-dimensional two-fluid flow without heat and mass transfer can be written as[6]:

$$\begin{aligned}
\frac{\partial}{\partial x}(\rho_1\alpha_1 u_1 u_1) &= -\alpha_1\frac{\partial p}{\partial x} + \frac{\partial}{\partial x}\left(\alpha_1\mu_1\frac{\partial u_1}{\partial x}\right) \\
\frac{\partial}{\partial x}(\rho_2\alpha_2 u_2 u_2) &= -\alpha_2\frac{\partial p}{\partial x} + \frac{\partial}{\partial x}\left(\alpha_2\mu_2\frac{\partial u_2}{\partial x}\right) \\
\frac{\partial}{\partial x}(\rho_1\alpha_1 u_1) &= 0 \\
\frac{\partial}{\partial x}(\rho_2\alpha_2 u_2) &= 0 \\
\alpha_1 + \alpha_2 &= 1
\end{aligned} \tag{1}$$

where a conventional single pressure approximation has been invoked. In what follows, each field's density and viscosity are assumed constant. For brevity, a factor of 4/3 is assumed embedded within the molecular viscosities.

As written, equation 1 employs no dynamic coupling (e.g., drag) between fields 1 and 2, other than a common pressure. This model system serves as a platform for developing the implicit method presented below. The influence of dynamic coupling terms due to drag, virtual mass and dispersion will be introduced. Also, the effects of mass transfer, alternate linearizations, multiple-dimensions, and multiple fields on stability are investigated.

Discretization

Equation 1 is written in vector form as:

$$R(Q) = \frac{\partial E}{\partial x} + \mathbf{B}\frac{\partial Q}{\partial x} + H = 0$$

$$Q \equiv (u_1, u_2, \alpha_1, \alpha_2, p)^T, \quad H \equiv (0, 0, 0, 0, \alpha_1 + \alpha_2 - 1)^T$$

$$E \equiv \begin{bmatrix} \rho_1\alpha_1 u_1 u_1 - \alpha_1\mu_1\dfrac{\partial u_1}{\partial x} \\ \rho_2\alpha_2 u_2 u_2 - \alpha_2\mu_2\dfrac{\partial u_2}{\partial x} \\ \rho_1\alpha_1 u_1 \\ \rho_2\alpha_2 u_2 \\ 0 \end{bmatrix}, \quad \mathbf{B} \equiv \begin{bmatrix} 0 & 0 & 0 & 0 & \alpha_1 \\ 0 & 0 & 0 & 0 & \alpha_2 \\ 0 & 0 & 0 & 0 & 0 \\ 0 & 0 & 0 & 0 & 0 \\ 0 & 0 & 0 & 0 & 0 \end{bmatrix} \tag{2}$$

A host of finite volume spatial discretization strategies can be applied. For the present work, in the momentum equations, second order central differencing is selected for pressure gradient and viscous terms and first order upwinding is employed for convection. In the volume fraction equations first order upwinding is used to evaluate cell face values of α, and central differencing with a conventional pressure weighted artificial dissipation term[7] is employed for cell face values of u. The rationale for this choice stems from analogy to pseudocompressibilty techniques[8], and is detailed below where comparison to single phase analysis is provided. Without loss of content in the development which follows, Δx is taken as constant, and u is assumed positive.

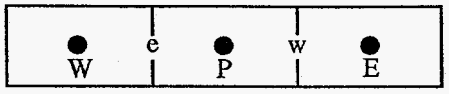

Figure 1. 1D control volumes on a Cartesian grid.

Referring to Figure 1, the discretization of equation 2 can be summarized as:

$$\frac{\partial}{\partial x}(\alpha u u) \rightarrow (E_{-x}\alpha)_e (E_{-x}u)_e (E_{-x}u)_e - (E_{-x}\alpha)_w (E_{-x}u)_w (E_{-x}u)_w$$

$$\frac{\partial}{\partial x}\left(\alpha\mu\frac{\partial u}{\partial x}\right) \rightarrow \mu\overline{(\alpha)}_e(\delta_x u)_e - \mu\overline{(\alpha)}_w(\delta_x u)_w \qquad (3)$$

$$\alpha\frac{\partial p}{\partial x} \rightarrow \alpha_P(\delta_{2x}p)_P$$

$$\frac{\partial}{\partial x}(\alpha u) \rightarrow (E_{-x}\alpha)_e (R_x u)_e - (E_{-x}\alpha)_w (R_x u)_w$$

where the operators used in equation 3 are defined as:

$$(E_{-x}\phi)_e \equiv \phi_P,\ \overline{(\phi)}_e \equiv (\phi_P + \phi_E)/2$$

$$(\delta_x\phi)_e \equiv (\phi_E - \phi_P)/\Delta x,\ (\delta_{2x}\phi)_P \equiv (\phi_E - \phi_W)/2\Delta x \qquad (4)$$

$$(R_x u)_e \equiv \overline{(u)}_e + \left(\frac{1}{\frac{2u}{\Delta x} + \frac{2v}{\Delta x^2}}\right)[\overline{(\delta_{2x}p)}_e - (\delta p)_e]$$

Implicit Solution Procedure

Applying an exact Newton linearization to equation 2 yields:

$$\mathbf{R'(Q)\Delta Q} = \mathbf{-R(Q)} \qquad (5)$$

where:

$$\mathbf{R'(Q)} = \frac{\partial}{\partial x}\mathbf{A}\bullet + \frac{\partial}{\partial Q}\left(\mathbf{B}\frac{\partial Q}{\partial x}\right) + \mathbf{C}$$

and Jacobians:

$$\mathbf{A} \equiv \frac{\partial E}{\partial Q},\ \frac{\partial}{\partial Q}\left(\mathbf{B}\frac{\partial Q}{\partial x}\right),\ \mathbf{C} \equiv \frac{\partial H}{\partial Q}$$

are given in the Appendix.

The spatial discretization, equations 3, is applied consistently on the RHS and LHS of equation 5. The fully implicit discrete linearized system to be solved becomes:

$$\mathbf{P}Q^{n+1} = S(Q^n) \qquad (6)$$

where, for notational simplicity in what follows, a non-Δ formulation is adopted. In equation 6, the block banded matrix **P** (tridiagonal with 5 x 5 blocks for 1D, two-field) corresponds to the discretization of $R'(Q^n)$, and $S(Q^n)$ corresponds to the discretization of $-R(Q^n) + R'(Q^n)\bullet Q^n$. For completeness, vectors $\mathbf{P}Q^{n+1}$ and $S(Q^n)$ are given in the Appendix. This basis scheme serves as a useful platform for investigating the effectiveness of solution strategies for solving the discrete system.

General Iterative Solution

A class of iterative schemes for the solution of equation 6 can be defined from:

$$\mathbf{M}Q^{n+1,k+1} = \mathbf{N}Q^{n+1,k} + S(Q^n) \qquad (7)$$

where

$$\mathbf{P} \equiv \mathbf{M} - \mathbf{N} \qquad (8)$$

represents the iterative splitting adopted.

To facilitate discussion of the preconditioning and iterative strategies developed below, **P** can be decomposed as:

$$\mathbf{P} = \mathbf{D} + (\mathbf{L} + \mathbf{U}) \qquad (9)$$

A decomposition of **D** is also introduced as:

$$\mathbf{D} \equiv \mathbf{D}_d + \mathbf{D}_o + \mathbf{D}_c \qquad (10)$$

where, for the linearization and discretization invoked, block diagonal matrix **D** is given in the Appendix and has the structure:

$$\mathbf{D} = \mathrm{diag}\begin{bmatrix} X & & X & & \\ & X & & X & \\ X & & X & & X \\ & X & & X & X \\ & & 1 & 1 & \end{bmatrix} \qquad (11)$$

$\mathbf{D}_d$ and $\mathbf{D}_o$ correspond to diagonal and off diagonal terms in rows 1-4 in each block of **D**. $\mathbf{D}_c$ contains only the row 5 entries corresponding to the compatibility condition, $\alpha_1 + \alpha_2 = 1$.

Time-Marching and Relaxation Formulations

Iterative procedures defined by equation 7 in general require some form of pseudo-time-stepping or under-relaxation, to obtain stability and/or optimum damping. A simple scalar relaxation procedure can be invoked:

$$\left(\mathbf{M} + \mathbf{D}_d\left(\frac{(1-\omega)}{\omega}\right)\right)Q^{k+1} = \mathbf{N}Q^k + S + \frac{(1-\omega)}{\omega}(\mathbf{D}_d)Q^k \qquad (12)$$

Equation 12 can be written as the equivalent time-marching scheme:

$$\Gamma_S\frac{\partial Q}{\partial t} + \mathbf{M}Q^{k+1} = \mathbf{N}Q^k + S \qquad (13)$$

by making the identification:

$$\Gamma_S = \frac{(1-\omega)}{\omega}\Delta t\mathbf{D}_d \qquad (14)$$

Alternatively, a block-relaxation procedure can be defined:

$$\left(\mathbf{M} + \mathbf{D}\left(\frac{(1-\omega)}{\omega}\right)\right)Q^{k+1} = \mathbf{N}Q^k + S + \frac{(1-\omega)}{\omega}(\mathbf{D})Q^k \qquad (15)$$

Equation 15 can be written as an equivalent time-marching scheme with block Jacobi preconditioning:

$$\Gamma_B \frac{\partial Q}{\partial t} + MQ^{k+1} = NQ^k + S \qquad (16)$$

by making the identification:

$$\Gamma_B = \frac{(1-\omega)}{\omega}\Delta t D \qquad (17)$$

In practice, the algebraic compatibility condition $\sum \alpha_l = 1$ is enforced exactly. Accordingly, $\mathbf{D}$ is replaced by $\mathbf{D} - \mathbf{D}_c$ in equations 15 and 17.

A relaxation convention is utilized in the authors' flow solver, and much of the discussion which follows below. This is because over-relaxation (i.e., $\omega > 1$ --> $\Delta t < 0$) provides optimum preconditioning for two of the schemes investigated, so the "unattractiveness" of utilizing a negative time-step is precluded. Also such an approach is consistent with the segregated pressure based forerunner to the present code. Equations 13 and 16 illustrate, however, that relaxation and time-marching approaches are identical.

Block Jacobi Schemes

For a block Jacobi iteration:

$$M_{BJ} \equiv D, N_{BJ} \equiv -(L+U) \qquad (18)$$

When used with block Jacobi preconditioning, this scheme (hereafter designated BP-BJ) is written:

$$\Gamma_B \frac{\partial Q}{\partial t} + DQ^{k+1} = -(L+U)Q^k + S \qquad (19)$$

A block Jacobi iteration with scalar relaxation (hereafter designated SP-BJ scheme) is written:

$$\Gamma_S \frac{\partial Q}{\partial t} + DQ^{k+1} = -(L+U)Q^k + S \qquad (20)$$

Block Gauss-Siedel Schemes

For a forward sweep block Gauss-Siedel scheme:

$$M_{FBGS} \equiv D + L, N_{FBGS} \equiv -U \qquad (21)$$

Analogous to equations 19 and 20, BP-BFGS and SP-BFGS schemes are defined:

$$\Gamma_B \frac{\partial Q}{\partial t} + (D+L)Q^{k+1} = -UQ^k + S \qquad (22)$$

$$\Gamma_S \frac{\partial Q}{\partial t} + (D+L)Q^{k+1} = -UQ^k + S \qquad (23)$$

In practice the forward sweep block Gauss-Siedel schemes are used in conjunction with symmetric backward sweeps, defined analogously to equations 22, 23. These symmetric schemes are designated BP-BSGS and SP-BSGS, below.

Stability Analysis

Equation 6 represents the fully implicit discrete system to be solved. Newton linearization and consistent LHS and RHS discretizations were employed in its derivation. Accordingly, in the stability analysis of the proposed iterative schemes, no contribution to the amplification matrices arises from inexact linearization or discretization inconsistencies.

Vector VonNeumann analysis is employed to investigate the stability characteristics of the four preconditioned systems defined by equations 19-20 and 22-23. These can be written in the common form:

$$G_1 Q^{k+1} = G_2 Q^k + S \qquad (24)$$

The iteration matrix associated with the general scheme defined by equation 24 is:

$$G \equiv G_1^{-1} G_2 \qquad (25)$$

The stability of the iterative schemes are assessed below by examining the eigenvalues of the Fourier symbol, $\hat{G} = \hat{G}_1^{-1}\hat{G}_2$, of their iteration matrix, G.

For a non-preconditioned, fully implicit scheme, $\hat{G} = \hat{P}$, where $\hat{P}$ is given in the Appendix. For the schemes considered, $\hat{G}_1$ and $\hat{G}_2$ can be easily constructed by splitting $\hat{P}$ appropriately, and applying the preconditioning operators used.

There are eight physical parameters which appear in the system: cell Reynolds numbers associated with each phase (Re_1, Re_2), density ratio (ρ_1/ρ_2), velocity ratio (u_1/u_2), field 1 volume fraction (α_1) and pressure and velocity gradient terms arising from the Newton linearization ($\delta_x u_j$, $\delta_{2x} p$). In what follows, stability characteristics are studied for the proposed iterative procedures applied to equation 6, for a range of physical parameters of interest.

A three-dimensional, four-field Navier-Stokes code, designated COMAC, which is based on the class of preconditioned iterative schemes introduced above, is under development by the authors. The vector Fourier analysis presented has been used to guide selection of iterative and preconditioning scheme, discretization and linearization. To understand the effects of physical boundary conditions, and to verify the results of the vector analysis, matrix stability results for COMAC are also included.

Block Jacobi Schemes

The Fourier iteration matrix associated with the BP-BJ scheme defined in equation 19 is $\hat{G}_{BP\text{-}BJ} = \hat{M}_{BP\text{-}BJ}\hat{N}_{BP\text{-}BJ}$. For this scheme, the stability characteristics given in Figure 2 are obtained. There, the spectral radius of the amplification matrix for the BP-BJ scheme is plotted vs. non-dimensional wave number.

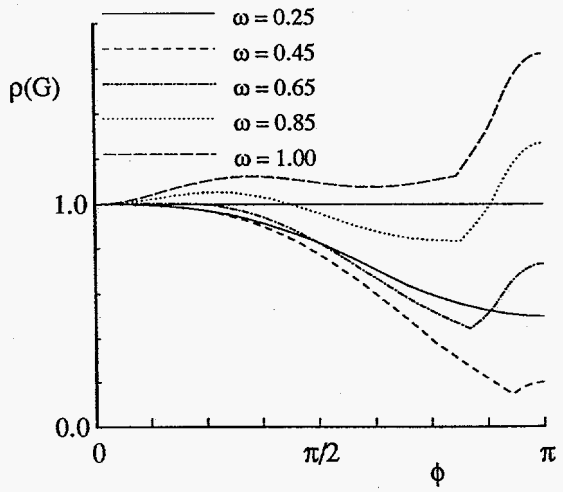

Figure 2. Stability of BP-BJ scheme.

The BP-BJ scheme is clearly conditionally stable for this case, where unity Reynolds numbers and zero

pressure and velocity gradients were assumed. An optimum relaxation factor of approximately $\omega = .45$ is observed, though this scheme exhibits significant stiffness at low wave numbers. The scheme is unstable for $\omega > .57$.

If scalar relaxation is used with the block Jacobi iteration (SP-BJ scheme defined by equation 20), the stability characteristics shown in Figure 3 are obtained.

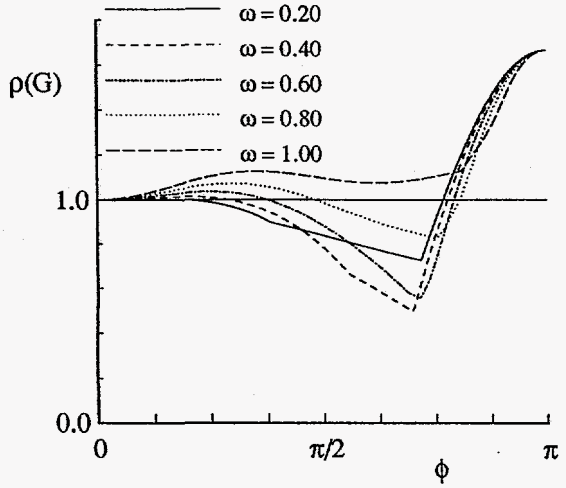

Figure 3. Stability of SP-BJ scheme

The SP-BJ scheme is observed to be unconditionally unstable.

Block Gauss-Siedel Schemes

Forward and backward block Gauss-Siedel schemes exhibit stability characteristics similar to block Jacobi. Specifically, both BP-BFGS and BP-BBGS schemes are conditionally stable, with $\omega_{opt} \cong 0.5$, and exhibit considerable low wave number stiffness. Also, both scalar preconditioned systems, SP-BFGS and SP-BBGS, are unconditionally unstable. For brevity, the stability plots for these four directionally biased schemes are not presented.

However, the construction of symmetric schemes from forward and backward block Gauss-Siedel component steps yields good damping properties. In Figure 4, $\rho(\hat{G}_{BP\text{-}BSGS})$, where $\hat{G}_{BP\text{-}BSGS} = \hat{G}_{BP\text{-}BBGS}\hat{G}_{BP\text{-}BFGS}$, is plotted vs. error phase. The BP-BSGS scheme alleviates much of the low wave number stiffness associated with the BP-BJ scheme. Optimum damping is achieved through over-relaxation, $\omega_{opt} \cong 1.3$. The BP-BSGS scheme remains stable to $\omega = 2.00$.

In Figure 5, the stability for the SP-BSGS scheme is plotted. Unlike the Jacobi and forward and backward sweep Gauss-Siedel schemes, scalar preconditioning does not yield an unconditionally unstable scheme when used for the symmetric Gauss-Siedel. Indeed, the damping characteristics of the SP-BSGS scheme are quite good. Optimum damping is achieved near $\omega_{opt} \cong 1.3$. However, the scheme becomes rapidly unstable at low wave numbers just above this optimum value ($\omega_{max} \cong 1.37$).

Of the four schemes investigated, BP-BSGS was chosen for further investigation, since it exhibits excellent damping properties and does not exhibit the potentially dangerous low wave number instability of SP-BSGS near its optimum damping rate.

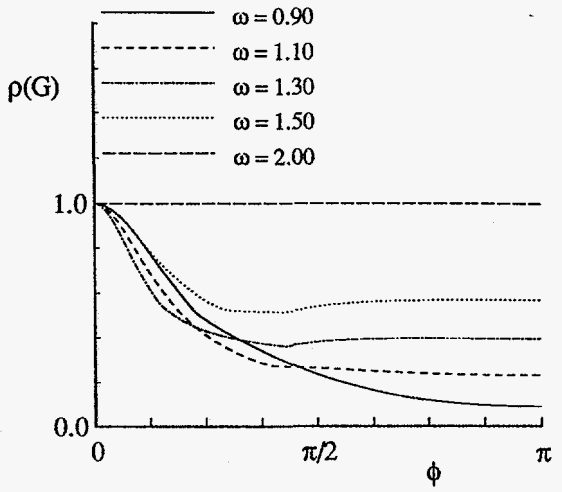

Figure 4. Stability of BP-BSGS scheme

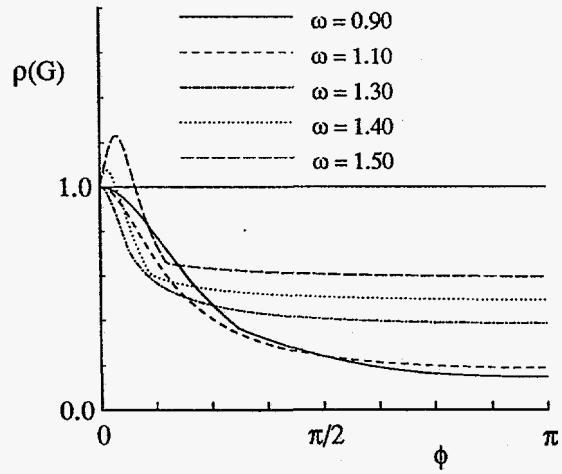

Figure 5. Stability of SP-BSGS scheme

Comparison with Single Phase

The lack of dynamic coupling in the basis scheme defined by equation 1, renders the two fields dynamically uncoupled. Indeed, the analyzed model equation represents the independent response of the uncoupled phases to the same pressure distribution. Accordingly, the stability results presented above are independent of density ratio (ρ_1/ρ_2), velocity ratio (u_1/u_2), and field 1 volume fraction (α_1). Consistent with this observation, the multi-field stability results correspond closely to those obtained for the discrete single phase analog to Equations 1. In particular, the eigenvalues of the basis two-field system contain as a subset, the eigenvalues arising in the single field system.

To illustrate this, Figure 6 shows an eigenvalue constellation for the BP-BSGS scheme ($\omega = 1.3$) applied to equation 6 with $R_{e1} = R_{e2} = 1.0$. Eleven modes ($-\pi < \phi < \pi$) were examined. At each wave number the two-field scheme returns four complex eigenvalues ($\lambda_5 = 0$, since compatibility is enforced without relaxation). The rank 2 single phase system returns two complex eigenvalues. As seen in Figure 6, these are equal to two of the four eigen-

values returned by the two-field system at the same wave number.

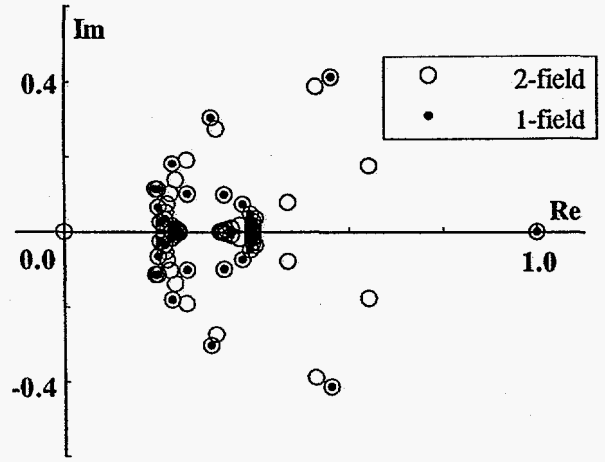

Figure 6. Comparison of two-field eigenvalues to one-field analog for BP-BSGS scheme.

Alternate Linearizations

A full Newton linearization must be maintained in the field continuity equations:

$$(\alpha u)^{n+1} \approx (\alpha^n u^{n+1}) + (u^n \alpha^{n+1}) \qquad (26)$$

"Frozen coefficient" linearization, i.e., $(\alpha u)^{n+1} \approx (u^n \alpha^{n+1})$, is singular in the coupled scheme (on inspection of **D**). The other alternative, $(\alpha u)^{n+1} \approx (\alpha^n u^{n+1})$, is singular unless a full Newton linearization is also employed for the momentum equations. In that case all four linear schemes are conditionally stable, but this non-standard linearization choice is catastrophic to the non-linear convergence procedure.

Despite this restriction on the continuity equations, a frozen coefficient linearization can be employed for the convection terms in the momentum equations, i.e., $(\alpha uu)^{n+1} \approx (\alpha^n u^n u^{n+1})$, with little effect on the linear performance of the scheme.

This is illustrated in Figure 7 which shows a comparison of full Newton and frozen coefficient linearizations on the stability of the 1D system for the BP-BSGS scheme ($\omega = 1.3$). Clearly the choice of momentum equation convection term linearization has little impact on the linear stability of the multi-fluid scheme.

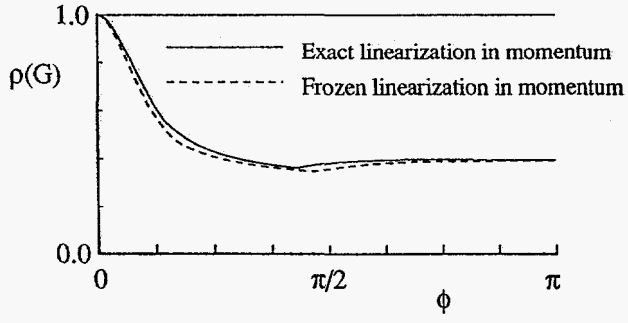

Figure 7. BP-BSGS stability for Newton and frozen coefficient linearization in the momentum equations.

Physical Parameters

Reynolds Number

The effect of cell Reynolds number on stability can be assessed by parameterizing the Reynolds numbers for the constituent fields. Figure 8a shows the stability plots for the BP-BSGS scheme ($\omega = 1.3$) for a range of Reynolds numbers ($R_{e1} = R_{e2}$) from 10^{-1} - 10^{10}. Clearly the effect of Reynolds number is a weak one, with only slightly deteriorated damping observed at infinite cell Reynolds numbers.

For small cell Reynolds numbers, the two additional eigenvalues per wave number which appear in the two-field system can be larger in magnitude than the two arising in the single field system. This feature of the two-field scheme is suggested in Figure 6. The damping deterioration associated with this phenomena is illustrated quantitatively in Figure 8b, which shows 1-ϕ stability plots for $R_{e1} = .1$, 1 and 10. Comparison with Figure 8a shows that the influence of the additional eigenvalues in the two-fluid system can significantly reduce the low wave number damping characteristics of the scheme at very low cell Reynolds numbers, but the effect is a weak one at $R_1 = 1$ and is undetectable at $R_{e1} = 10$.

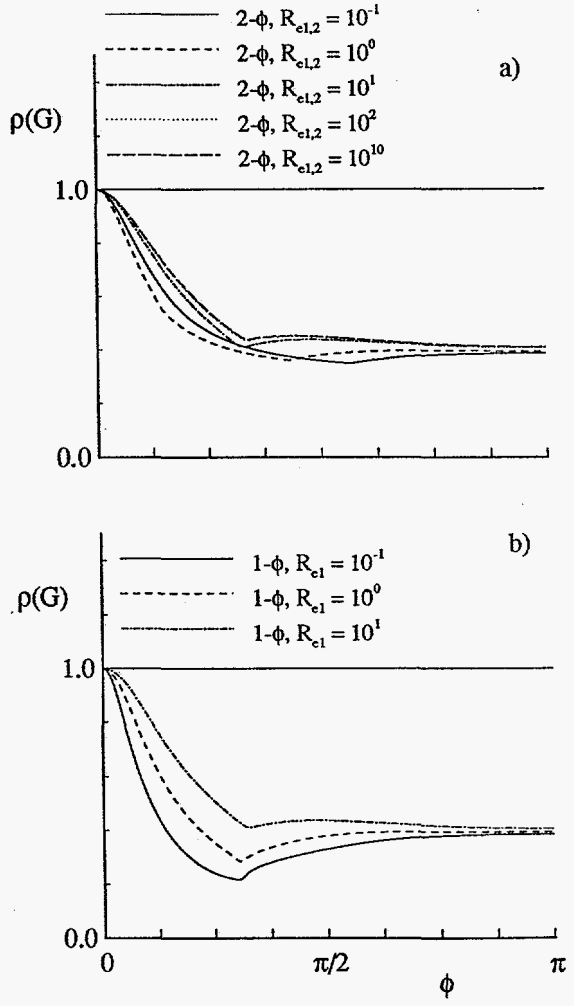

Figure 8. BP-BSGS stability for a range of cell Reynolds numbers. a) two-field, b) one-field.

Inter-field Transfer

The introduction of interfacial dynamics and mass transfer couples the constituent fields. The impact of such terms on the physics of the flow and stability of the algorithm becomes dependent on the density ratio (ρ_1/ρ_2), velocity ratio (u_1/u_2), and field 1 volume fraction (α_1). Therefore, in order to meaningfully parameterize the stability of inter-field transfer terms, relevant engineering scales are adopted for these three flow parameters, and the field Reynolds numbers. In particular, for high pressure steam-water boiling heat exchanger systems, the choices $\rho_1/\rho_2 = 10$, $u_1/u_2 = .5$ and $\alpha_1 = .5$ are relevant (hereafter designated HPW). For "bubbly" air-water flows, the choices $\rho_1/\rho_2 = 1000$, $u_1/u_2 = 0.8$ and $\alpha_1 = .95$ are relevant (hereafter designated BAW). Typically, cell Reynolds numbers of $> 10^1$ are deployed in practical engineering computations. The values $R_{e1} = R_{e2} = 10$ are used below.

The most commonly employed models for interfacial momentum transfer are drag, virtual mass and dispersion. The stability characteristics of these forces, and mass transfer, are each treated below. The augmentation of the Fourier symbol, $\hat{P}$, arising from implicit treatment of these interfacial coupling terms is $\hat{P} \Rightarrow \hat{P} + \hat{P}_{IC}$, where $\hat{P}_{IC}$ is given in the Appendix.

Drag

Drag is incorporated within the momentum equations as:

$$\begin{aligned} M1 &\Rightarrow M1 + D(u_2 - u_1) \\ M2 &\Rightarrow M2 + D(u_1 - u_2) \end{aligned} \tag{27}$$

where M1 and M2 denote the momentum equations in the baseline formulation (equations 1). Drag is incorporated within the momentum equation interpolation procedure used for facial flux reconstruction[3] and, therefore, appears in the operator R_x (equations 4, A.5). D is generally modelled for all interfaces as:

$$D = C_D \rho_c |u_1 - u_k| A_i''' \tag{28}$$

where C_D is the drag coefficient, ρ_c is the "carrier" field density, and A_i''' the interfacial area density. A practical range for drag parameterization is defined from:

$$0 \le D^* \equiv \frac{D}{\rho_c |u_2 - u_1| \alpha_2 / \Delta x} \le 1 \tag{29}$$

Figure 9 shows a comparison of the effect of drag on the damping properties of the BP-BSGS scheme ($\omega = 1.3$). In this plot, the two sets of physical scales introduced above (HPW, BAW) are used, and $R_{e1} = R_{e2} = 10$.The scheme remains stable in the physically relevant range $D^* < 1$. Indeed, the influence of drag is small, though extremely large values of drag (viz., unrealistic values as may occur in early iteration) have been observed to destabilize the scheme.

Mass Transfer

Mass transfer is incorporated within the momentum and continuity equations as:

$$\begin{aligned} M1 &\Rightarrow M1 + \Gamma^{21} u_2 - \Gamma^{12} u_1 \\ M2 &\Rightarrow M2 + \Gamma^{12} u_1 - \Gamma^{21} u_2 \\ C1 &\Rightarrow C1 + \Gamma^{21} - \Gamma^{12} \\ C2 &\Rightarrow C2 + \Gamma^{12} - \Gamma^{21} \end{aligned} \tag{30}$$

where C1 and C2 denote the continuity equations in the baseline formulation (equations 1). Here Γ^{mn} are mass transfer rates from field m to field n in kg/m^3s, defined such that $\Gamma^{mn} \ge 0$. These terms are similar to drag, but are non-symmetric, and, appear in the continuity equations. For $\Gamma^{mn} \approx \Gamma^{nm}$, the impact of mass transfer is similar to drag, so the non-symmetric cases are considered here. For the case where $\Gamma^{nm} = 0$, the maximum physically plausible value of Γ^{mn} to be considered can be estimated from realizability constraints (i.e., $\alpha^{n+1} \ge 0$) to be:

$$\Gamma^{mn*} \equiv \frac{\Gamma^{mn}}{\rho_m u_m \alpha_m / \Delta x} \le 1 \tag{31}$$

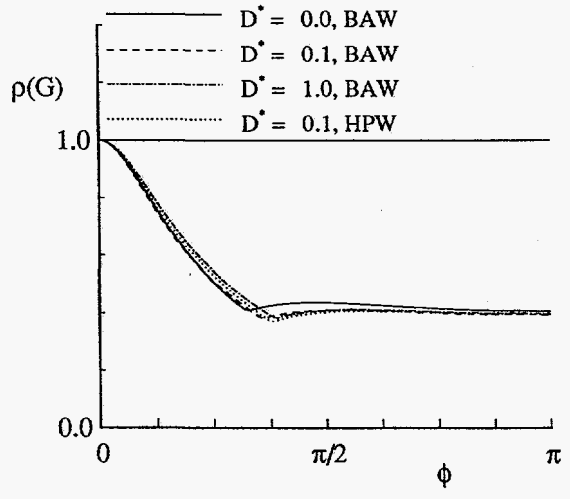

Figure 9. BP-BSGS stability for a range of nondimensional drag.

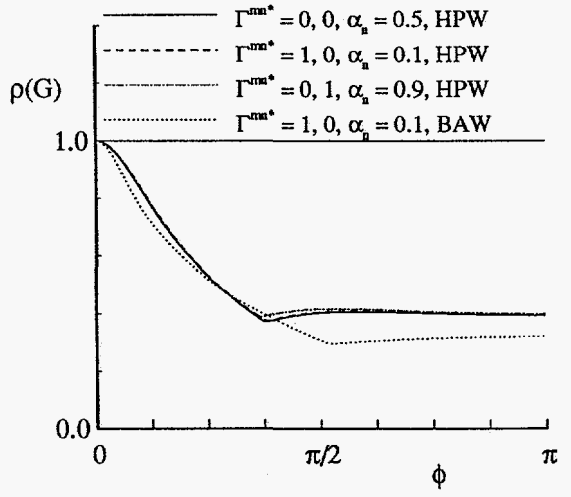

Figure 10. BP-BSGS stability for a range of nondimensional mass transfer.

Figure 10 illustrates that values of Γ^{mn*} at the realizability limit do not significantly affect the linear stability of the scheme, even at high density ratio. For these results, small values of donor field volume fraction are taken, ($\alpha_n = .05$), consistent with the realizability limit. Other scales are taken as above (i.e., HPW, BAW, $R_{e1} = R_{e2} = 10$, $D^* = 0$).

Dispersion

Dispersion is incorporated within the momentum equations as:

$$M1 \Rightarrow M1 + C_T\rho_1(u_2-u_1)^2\frac{\partial\alpha^2}{\partial x}$$
$$M1 \Rightarrow M1 - C_T\rho_1(u_2-u_1)^2\frac{\partial\alpha^2}{\partial x} \qquad (32)$$

Physically reasonable values of dispersion coefficient are $C_T \le 1.0$. As with drag and mass transfer, the influence of these terms on the stability of the linear scheme was found to be small (plot not included for brevity).

Virtual Mass

Virtual mass is incorporated within the momentum equations as:

$$M1 \Rightarrow M1 - C_V\alpha_2\rho_1\left[u_1\frac{\partial u_1}{\partial x} - u_2\frac{\partial u_2}{\partial x}\right]$$
$$M2 \Rightarrow M2 - C_V\alpha_2\rho_1\left[u_2\frac{\partial u_2}{\partial x} - u_1\frac{\partial u_1}{\partial x}\right] \qquad (33)$$

Considering the case of no mass transfer, equation 33 can be manipulated to yield modified effective convection terms in the two momentum equations:

$$\frac{\partial}{\partial x}(\rho_1\alpha_1u_1u_1) \Rightarrow \left[1+C_V\left(\frac{\alpha_2}{\alpha_1}\right)\right]\frac{\partial}{\partial x}(\rho_1\alpha_1u_1u_1) - \left[C_V\left(\frac{\rho_1}{\rho_2}\right)\right]\frac{\partial}{\partial x}(\rho_2\alpha_2u_2u_2)$$
$$\frac{\partial}{\partial x}(\rho_2\alpha_2u_2u_2) \Rightarrow \left[1+C_V\left(\frac{\rho_1}{\rho_2}\right)\right]\frac{\partial}{\partial x}(\rho_2\alpha_2u_2u_2) - \left[C_V\left(\frac{\alpha_2}{\alpha_1}\right)\right]\frac{\partial}{\partial x}(\rho_1\alpha_1u_1u_1) \qquad (34)$$

Physically reasonable values of virtual mass coefficient are $C_V \le 0.5$. For low density ratio scales (HPW), a fully implicit treatment of virtual mass (i.e., all four terms on the RHS of equation 34 appearing in $\hat{P}_{IC}$), has only minor impact on the linear stability of the BP-BSGS scheme. This is illustrated in Figure 11a. Here, the standard HPW scales are taken as above with $D^* = 0.1$ and $C_T = 0.1$.

At high density ratios (BAW) the fully implicit treatment can be destabilizing to the linear scheme, though retaining only the virtual mass terms which contribute to the diagonal of $\hat{P}_{IC}$ stabilizes it. These observations are illustrated in Figure 11b. The impact of this semi-implicit treatment on the non-linear performance of the code is not yet known.

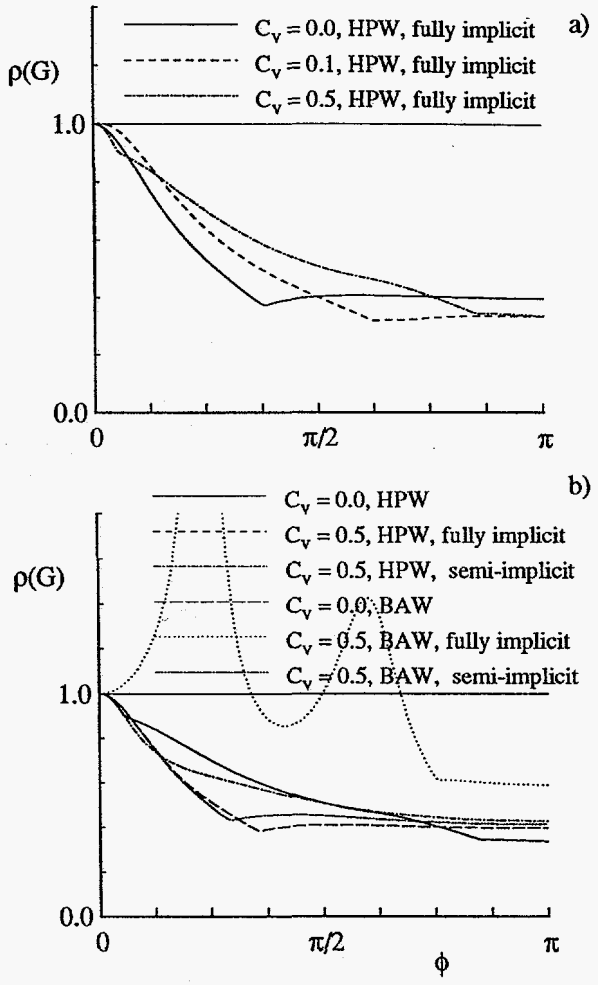

Figure 11. BP-BSGS stability for a range of virtual mass coefficients and linearization strategies.

Comparison of Vector and Matrix Stability

To illustrate the validity of the foregoing vector stability analyses, and to investigate the effect of physical boundary conditions on the scheme, a matrix stability analysis was performed. The platform for the matrix analysis is the authors' multi-fluid Navier-Stokes code, COMAC, which utilizes the BP-BSGS scheme introduced above.

A vertical air-water bubbly flow is investigated. Here, problem parameters were set at: $\rho_1 = 1000$ kg/m^3, $\rho_2 = 1$ kg/m^3, $\mu_1 = 10^{-3}$ kg/ms, $\mu_2 = 10^{-5}$ kg/ms, $\Delta x = 0.05$ m, ni = 20 (i.e., L = 1.0 m, 20 cells). A simple bubble drag model due to Wallis[9] was employed:

$$D = \frac{1}{8}C_D\rho_1|u_2-u_1|\frac{6\alpha_2}{D_b},\quad C_D \equiv \frac{6.3}{R_{eb}^{0.385}},\quad R_{eb} \equiv \frac{\rho_1|u_2-u_1|2D_b}{\mu_1} \qquad (35)$$

The flow solver's response to a given set of initial conditions, $u_1 = 1.0$ m/s, $u_2 = 1.1$ m/s, $\alpha_1 = 0.9$, $\alpha_2 = 0.1$ was studied. A bubble radius of $D_b = 1.0$ mm was set. A frozen coefficient linearization was used in the momentum equations and ω was set to 0.8 (equation 17).

Figure 12a shows that if periodic boundary conditions are applied, COMAC returns iteration matrix eigenvalues which are coincident with those returned by the Fourier stability analysis. If conventional duct flow boundary conditions are applied (inlet: u_1, u_2, α_1, α_2 fixed, $dp/dx = 0$; exit: p fixed, $du_1/dx = du_2/dx = d\alpha_1/dx = d\alpha_2/dx = 0$), the eigenvalue spectrum is modified as shown.

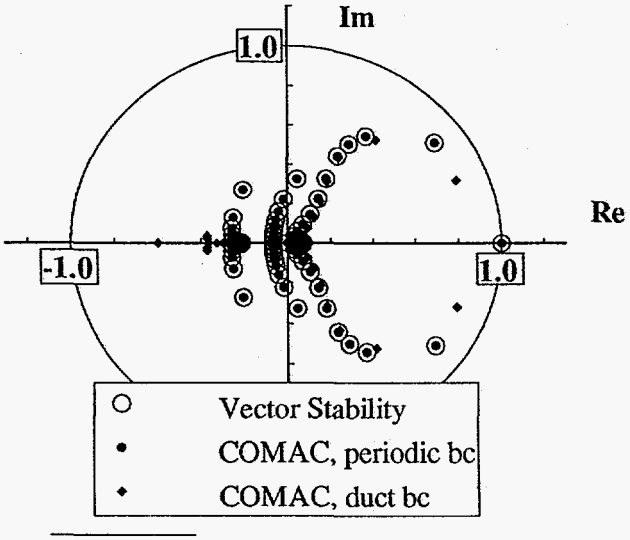

Figure 12a. Comparison of vector and matrix analyses for an air water bubbly flow.

Figure 12b shows corresponding linear solver convergence rates for these two COMAC runs at the first nonlinear iteration (corresponding to Figure 12a). The application of physical boundary conditions are observed to improve damping of the scheme somewhat.

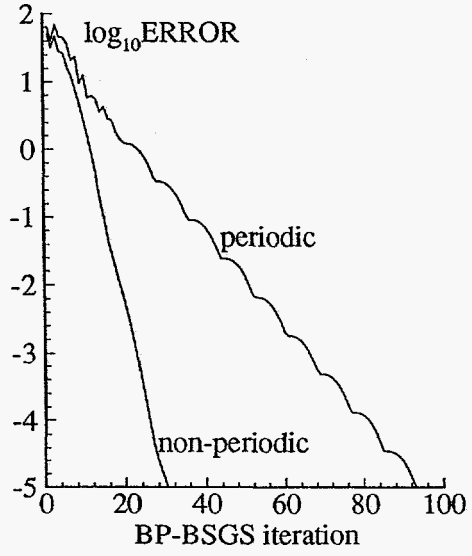

Figure 12b. Comparison of BP-BSGS convergence histories for periodic and duct flow boundary conditions

Extension to Multiple Fields

The analyses presented above for two-fields extend readily to an arbitrary number of fields. As each new field is introduced to the basis scheme, two new eigenvalues appear, corresponding to the additional momentum and continuity equations. These eigenvalues are identical to the two additional obtained in extending the single field to a two-field system. Accordingly, the n-field system exhibits identical stability characteristics to the two-field system.

Extension to Multiple Dimensions

The stability analyses presented above for one-dimension can also be readily extended to multiple dimensions. For two-fields, the resulting Fourier eigensystem is of rank 7. Figure 13 shows examples of 2D stability results obtained for the BP-BSGS scheme, with no interfacial transfer terms. Taking $u = v$, $R_{e1} = R_{e2} = 10^6$, cell aspect ratio, $AR = \Delta x/\Delta y = 1.0$, and $\omega = 0.8$, the results in Figure 13a are obtained. There it is observed that the 2D scheme exhibits good damping characteristics at all wave numbers away from the origin, consistent with the observations made above for the 1D scheme.

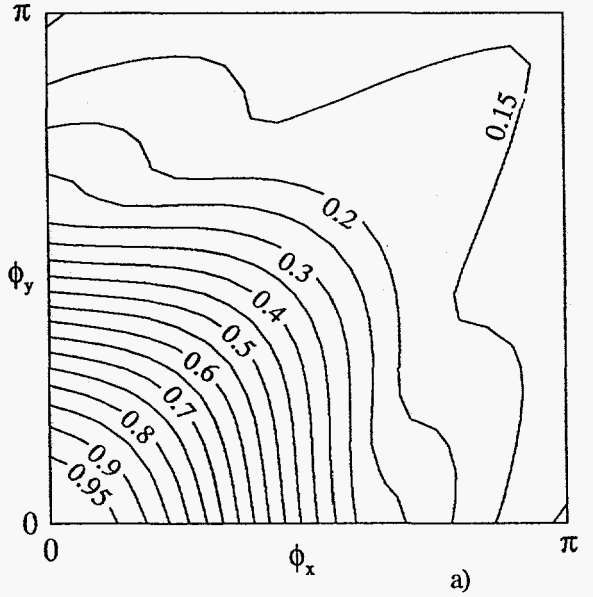

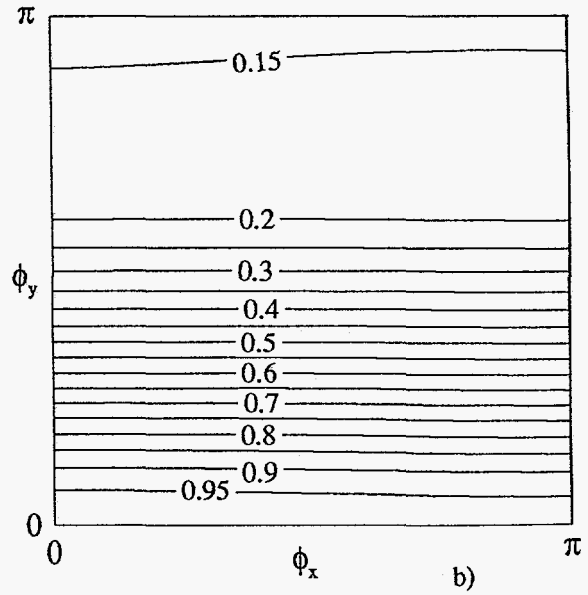

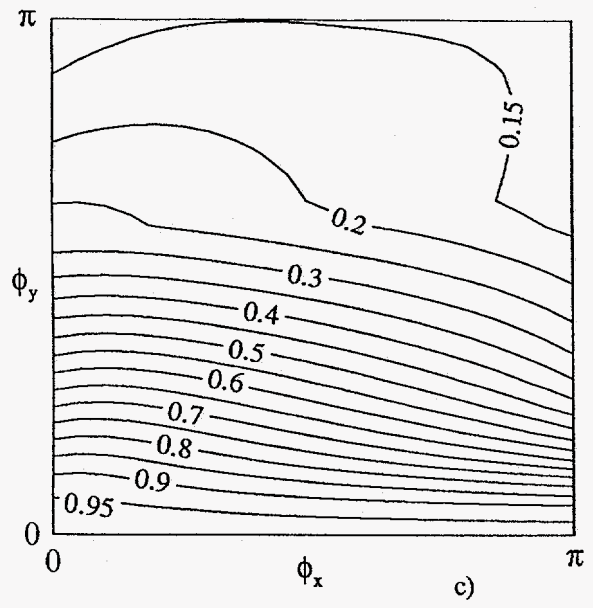

Figure 13. Two-dimensional stability results for BP-BSGS scheme. a) u = v, AR = 1, b) u = v, AR = 100, c) u = 100v, AR = 100.

On high aspect ratio grids, as are characteristic of high L/D_H boiling heat exchanger geometries, long wavelength axial modes become poorly damped. This is illustrated in Figure 13b where a grid aspect ratio of 100 was used. In such geometries, the transverse velocity usually scales with the axial velocity. Accordingly, if v is taken to be equal to u/AR, the stability plot presented in Figure 13c is obtained. There it is observed that the "well guided" nature of the flow can introduce some moderate additional transverse mode stiffness.

The low axial wave number stiffness observed on high aspect ratio grids for the BP-BSGS scheme can be effectively handled by deploying coupled block correction strategies[5], or a semi-coarsened algebraic multigrid procedure.

Conclusion

A new implicit method, developed for the solution of the viscous full multi-fluid equations has been presented. Stability analyses were performed for preconditioned iterative schemes applied to the coupled discrete system of equations which arise in the formulation.

Several conclusions are drawn in the work including: (1) A block symmetric Gauss-Siedel scheme with block Jacobi preconditioning (BP-BSGS) gives rise to very good damping properties for the multi-fluid system. Optimal convergence rates for this scheme can be obtained with successive over-relaxation. (2) Conditional stability requires that a minimum level of exactness be employed in developing an approximate Newton linearization for the continuity equations. An exact linearization in the momentum equations affords no benefit to the linear stability of the scheme compared to a "frozen" coefficient linearization. (3) In the absence of inter-field transfer terms, the basis multi-fluid scheme exhibits very similar stability characteristics to its single phase analog. Only at very low cell Reynolds numbers does the multi-fluid system exhibit deteriorated damping properties compared to single phase. (4) Reynolds number effects are moderate; the limit of infinite cell Reynolds numbers marginalizes the stability of the scheme only slightly. (5) Implicit treatment of several investigated interfacial transfer mechanisms (mass transfer, drag, dispersion and virtual mass) can affect the stability of the scheme, but the BP-BSGS scheme analyzed retains good damping characteristics for physically realistic values of these modelled terms. (6) A multi-fluid Navier-Stokes code which deploys the BP-BSGS scheme was used. Comparison of vector and matrix stability verified the correctness of the vector analyses presented and demonstrated that physical boundary conditions can benefit the damping characteristics of the scheme. (7) The two-dimensional stability characteristics of the scheme are consistent with one-dimensional results, with high aspect ratio grids introducing diminished low wave number axial mode damping, as commonly observed in most CFD algorithms.

References

1) Stewart, H. B., Wendroff, B. (1984) "Two-Phase Flow: Models and Methods," Journal of Computational Physics, Vol. 56, p. 363.

2) No, H. C., Kazimi, M. S. (1985) "Effects of Virtual Mass on the Mathematical Stability of the Two-Fluid Model," Nuclear Science and Engineering, Vol. 89, p. 197.

3) Lee, J. Y., No, H. C. (1991) "Effect of Intefacial Drag on the Numerical Stability of the Two-Step Method in the Two-Fluid Model," Nuclear Engineering and Design, Vol. 126, p. 427.

4) Spalding, D. B. (1980) "Mathematical Methods in Nuclear-Reactor Thermal Hydraulics," Keynote Paper, ANS Meeting on Nuclear-Reactor Thermal Hydraulics, Saratoga, NY.

5)Kunz, R. F., Siebert, B. W., Cope, W. K., Foster, N. F., Antal, S. P., Ettorre S. M. (1997), "A Coupled Phasic Exchange Algorithm for Three-Dimensional Multi-Field Analysis of Heated Flows with Mass Transfer", Submitted to International Journal of Multiphase Flow.

6) Ishii, M., (1975) Thermo-Fluid Dynamic Theory of Two-Phase Flow, Eyrolles, Paris.

7) Rhie, C. M., Chow, W. L. (1983) "Numerical Study of the Turbulent Flow Past an Airfoil with Trailing Edge Separation," AIAA Journal, Vol. 21, p. 1527.

8) Venkateswaran, S., Tamamidis, P., Merkle, C. L. (1996) "Interpretation of Pressure-Based Methods as Time-Marching Schemes," Proceedings of the 15th International Conference on Numerical Methods in Fluid Dynamics, Springer-Verlag.

9) Wallis G. B. (1969) One Dimensional Two-Phase Flow, McGraw-Hill, New York.

Appendix

$$\mathbf{A} \equiv \frac{\partial \mathbf{E}}{\partial \mathbf{Q}} = \begin{bmatrix} 2\rho_1\alpha_1 u_1 - \mu_1\alpha_1\frac{\partial}{\partial x} & 0 & \rho_1 u_1 u_1 - \mu_1\frac{\partial u_1}{\partial x} & 0 & 0 \\ 0 & 2\rho_2\alpha_2 u_2 - \mu_2\alpha_2\frac{\partial}{\partial x} & 0 & \rho_2 u_2 u_2 - \mu_2\frac{\partial u_2}{\partial x} & 0 \\ \rho_1\alpha_1 & 0 & \rho_1 u_1 & 0 & 0 \\ 0 & \rho_2\alpha_2 & 0 & \rho_2 u_2 & 0 \\ 0 & 0 & 0 & 0 & 0 \end{bmatrix} \tag{A.1}$$

$$\frac{\partial}{\partial \mathbf{Q}}\left(\mathbf{B}\frac{\partial \mathbf{Q}}{\partial x}\right) = \begin{bmatrix} 0\ 0\ \frac{\partial p}{\partial x}\ 0\ \alpha_1\frac{\partial}{\partial x}\bullet \\ 0\ 0\ 0\ \frac{\partial p}{\partial x}\ \alpha_2\frac{\partial}{\partial x}\bullet \\ 0\ 0\ 0\ 0\ 0 \\ 0\ 0\ 0\ 0\ 0 \\ 0\ 0\ 0\ 0\ 0 \end{bmatrix}, \quad \mathbf{C} \equiv \frac{\partial \mathbf{H}}{\partial \mathbf{Q}} = \begin{bmatrix} 0\ 0\ 0\ 0\ 0 \\ 0\ 0\ 0\ 0\ 0 \\ 0\ 0\ 0\ 0\ 0 \\ 0\ 0\ 0\ 0\ 0 \\ 0\ 0\ 1\ 1\ 0 \end{bmatrix}$$

$$\mathbf{PQ}^{n+1} = \begin{Bmatrix} [2\rho_1 E_{-x}\alpha_1^n E_{-x}u_1^n E_{-x}u_1^{n+1}]_{cw} + [\rho_1 E_{-x}u_1^n E_{-x}u_1^n E_{-x}\alpha_1^{n+1}]_{ew} - [\mu_1\overline{\alpha_1^n}\delta_x u_1^{n+1}]_{ew} - [\mu_1\delta_x u_1^n\overline{\alpha_1^{n+1}}]_{ew} + [\delta_{2x}p^n\alpha_1^{n+1}]_P + [\alpha_1^n\delta_{2x}p^{n+1}]_P \\ [2\rho_2 E_{-x}\alpha_2^n E_{-x}u_2^n E_{-x}u_2^{n+1}]_{cw} + [\rho_2 E_{-x}u_2^n E_{-x}u_2^n E_{-x}\alpha_2^{n+1}]_{ew} - [\mu_2\overline{\alpha_2^n}\delta_x u_2^{n+1}]_{ew} - [\mu_2\delta_x u_2^n\overline{\alpha_2^{n+1}}]_{ew} + [\delta_{2x}p^n\alpha_2^{n+1}]_P + [\alpha_2^n\delta_{2x}p^{n+1}]_P \\ [\rho_1 E_{-x}\alpha_1^n R_x u_1^{n+1}]_{ew} + [\rho_1 R_x u_1^n E_{-x}\alpha_1^{n+1}]_{ew} \\ [\rho_2 E_{-x}\alpha_2^n R_x u_2^{n+1}]_{ew} + [\rho_2 R_x u_2^n E_{-x}\alpha_2^{n+1}]_{ew} \\ \alpha_1^{n+1} + \alpha_2^{n+1} \end{Bmatrix} \tag{A.2}$$

$$S(Q^n) = \begin{Bmatrix} [\rho_1 E_{-x}\alpha_1^n E_{-x}u_1^n E_{-x}u_1^n]_{ew} - [\mu_1\overline{\alpha_1^n}\delta_x u_1^n]_{ew} + [\delta_{2x}p^n\alpha_1^n]_P \\ [\rho_2 E_{-x}\alpha_2^n E_{-x}u_2^n E_{-x}u_2^n]_{ew} - [\mu_2\overline{\alpha_2^n}\delta_x u_2^n]_{ew} + [\delta_{2x}p^n\alpha_2^n]_P \\ [\rho_1 E_{-x}\alpha_1^n R_x u_1^n]_{ew} \\ [\rho_2 E_{-x}\alpha_2^n R_x u_2^n]_{ew} \\ 1 \end{Bmatrix}$$

where $[\ ]_{ew}$ designates $(\ )_e - (\ )_w$

$$\mathbf{D} = \text{diag}\begin{bmatrix} 2\rho_1 E_{-x}\alpha_{1e}^n E_{-x}u_{1e}^n + \frac{\mu_1}{\Delta x}[\overline{\alpha_{1e}^n} + \overline{\alpha_{1w}^n}] & 0 & \rho_1 E_{-x}u_{1e}^n E_{-x}u_{1e}^n - \frac{\mu_1}{2}[\delta_x u_{1e}^n - \delta_x u_{1w}^n] + \delta_{2x}p_P^n & 0 & 0 \\ 0 & 2\rho_2 E_{-x}\alpha_{2e}^n E_{-x}u_{2e}^n + \frac{\mu_2}{\Delta x}[\overline{\alpha_{2e}^n} + \overline{\alpha_{2w}^n}] & 0 & \rho_2 E_{-x}u_{2e}^n E_{-x}u_{2e}^n - \frac{\mu_2}{2}[\delta_x u_{2e}^n - \delta_x u_{2w}^n] + \delta_{2x}p_P^n & 0 \\ \frac{\rho_1}{2}(E_{-x}\alpha_{1e}^n - E_{-x}\alpha_{1w}^n) & 0 & \rho_1 R_x u_{1e}^n & 0 & \frac{3\rho_1}{4}[\kappa_{1e}E_{-x}\alpha_{1e}^n + \kappa_{1w}E_{-x}\alpha_{1w}^n] \\ 0 & \frac{\rho_2}{2}(E_{-x}\alpha_{2e}^n - E_{-x}\alpha_{2w}^n) & 0 & \rho_2 R_x u_{2e}^n & \frac{3\rho_2}{4}[\kappa_{2e}E_{-x}\alpha_{2e}^n + \kappa_{2w}E_{-x}\alpha_{2w}^n] \\ 0 & 0 & 1 & 1 & 0 \end{bmatrix} \tag{A.3}$$

where

$$\kappa_{1f} = \overline{\left(1/\left[2u_1 + \frac{2\nu_1}{\Delta x}\right]\right)_f}$$

$$\hat{\mathbf{P}} = \begin{bmatrix} 2\rho_1\alpha_1 u_1(1-e^{-i\phi}) - \left(\frac{\mu_1\alpha_1}{\Delta x}\right)(e^{i\phi}-2+e^{-i\phi}) & 0 & \rho_1 u_1 u_1(1-e^{-i\phi}) - \left(\frac{\mu_1\delta_x u_1}{2}\right)(e^{i\phi}-e^{-i\phi}) + \delta_{2x}p & 0 & \left(\frac{\alpha_1}{2}\right)(e^{i\phi}-e^{-i\phi}) \\ 0 & 2\rho_2\alpha_2 u_2(1-e^{-i\phi}) - \left(\frac{\mu_2\alpha_2}{\Delta x}\right)(e^{i\phi}-2+e^{-i\phi}) & 0 & \rho_2 u_2 u_2(1-e^{-i\phi}) - \left(\frac{\mu_2\delta_x u_2}{2}\right)(e^{i\phi}-e^{-i\phi}) + \delta_{2x}p & \left(\frac{\alpha_2}{2}\right)(e^{i\phi}-e^{-i\phi}) \\ \frac{\rho_1\alpha_1}{2}(e^{i\phi}-e^{-i\phi}) & 0 & \rho_1 u_1(1-e^{-i\phi}) & 0 & \left(\frac{\alpha_1}{4}\right)\kappa_1\hat{R} \\ 0 & \frac{\rho_2\alpha_2}{2}(e^{i\phi}-e^{-i\phi}) & 0 & \rho_2 u_2(1-e^{-i\phi}) & \left(\frac{\alpha_2}{4}\right)\kappa_2\hat{R} \\ 0 & 0 & 1 & 1 & 0 \end{bmatrix} \tag{A.4}$$

$$\hat{\mathbf{P}}_{IC} = \begin{bmatrix} \left(D\Delta x + \Gamma^{12} + C_V\left(\frac{\alpha_2}{\alpha_1}\right)2\rho_1\alpha_1 u_1(1-e^{-i\phi})\right) & \left(-D\Delta x - \Gamma^{21} - C_V\left(\frac{\rho_1}{\rho_2}\right)2\rho_2\alpha_2 u_2(1-e^{-i\phi})\right) & \left(C_V\left(\frac{\alpha_2}{\alpha_1}\right)\rho_1 u_1 u_1(1-e^{-i\phi})\right) & \left(-\frac{C_T\rho_1(u_2-u_1)^2}{2}(e^{i\phi}-e^{-i\phi}) - C_V\left(\frac{\rho_1}{\rho_2}\right)\rho_2 u_2 u_2(1-e^{-i\phi})\right) & 0 \\ \left(-D\Delta x - \Gamma^{12} - C_V\left(\frac{\alpha_2}{\alpha_1}\right)2\rho_1\alpha_1 u_1(1-e^{-i\phi})\right) & \left(D\Delta x + \Gamma^{21} + C_V\left(\frac{\rho_1}{\rho_2}\right)2\rho_2\alpha_2 u_2(1-e^{-i\phi})\right) & \left(-C_V\left(\frac{\alpha_2}{\alpha_1}\right)\rho_1 u_1 u_1(1-e^{-i\phi})\right) & \left(\frac{C_T\rho_1(u_2-u_1)^2}{2}(e^{i\phi}-e^{-i\phi}) + C_V\left(\frac{\rho_1}{\rho_2}\right)\rho_2 u_2 u_2(1-e^{-i\phi})\right) & 0 \\ 0 & 0 & 0 & 0 & \left(\frac{\alpha_1}{4}\right)\kappa_{1IC}\hat{R} \\ 0 & 0 & 0 & 0 & \left(\frac{\alpha_2}{4}\right)\kappa_{2IC}\hat{R} \\ 0 & 0 & 0 & 0 & 0 \end{bmatrix} \tag{A.5}$$

where $\kappa_{1IC} = 1/\left[2u_1 + \frac{2\nu_1}{\Delta x} + \frac{D\Delta x}{\alpha_1\rho_1} + \frac{\Gamma^{12}\Delta x}{\alpha_1\rho_1}\right]$, $\kappa_{2IC} = 1/\left[2u_2 + \frac{2\nu_2}{\Delta x} + \frac{D\Delta x}{\alpha_2\rho_2} + \frac{\Gamma^{21}\Delta x}{\alpha_2\rho_2}\right]$,

$$\hat{R} = (e^{2i\phi} - 4e^{i\phi} + 6 - 4e^{-i\phi} + e^{-2i\phi})$$